First-principles infra-red spectrum of nitric acid and nitric acid monohydrate crystals

ARTICLE · OCTOBER 2004

CITATION
1

READS
21

4 AUTHORS, INCLUDING:

Thomas Archer
Trinity College Dublin
23 PUBLICATIONS **428** CITATIONS

SEE PROFILE

First-Principles Infrared Spectrum of Nitric Acid and Nitric Acid Monohydrate Crystals

Delia Fernández-Torre* and Rafael Escribano

Instituto de Estructura de la Materia, C.S.I.C., Serrano 123, 28006 Madrid, Spain

Tom Archer, J. M. Pruneda, and Emilio Artacho

Department of Earth Sciences, University of Cambridge, Downing Street, Cambridge CB2 3EQ, U.K.

Received: June 24, 2004; In Final Form: September 3, 2004

The spectra of nitric acid and nitric acid monohydrate crystals, including both vibration frequencies and infrared intensities, have been calculated from first principles using the methodology developed for the SIESTA program. In this method, infrared intensities are evaluated from the macroscopic polarization changes with atomic displacements per normal mode. The process requires the calculation of Born charges associated with atomic displacements. The actual value of the Born tensor elements gives interesting information on the electronic nature of the bonds. The application of this method to the two systems of atmospheric relevance studied here is particularly interesting. The calculated spectra are compared to previous experimental transmission spectra of these species with overall satisfactory agreement. The calculations provide a useful tool for the interpretation and assignment of the observed spectra.

Introduction

The simulation of infrared spectra of condensed materials by theoretical methods is not an easy task. As far as we know, previous ab initio simulations have been carried out along either of the following schemes. In molecular dynamics calculations, most frequently using the Car−Parrinello method (CPMD), the macroscopic polarization of the solid is evaluated at each step of a trajectory, and then the dipole−dipole correlation function, which is directly related to the infrared absorbance, is evaluated. This method is specially suitable when dealing with liquids or anharmonic systems in general, such as solids at high temperatures. The second method exploits the harmonic approximation and is thus best suited for solids or molecules at low temperatures. It requires the calculation of the vibrational frequencies, by diagonalization of the dynamical matrix, and the Born effective-charge tensor. These two quantities are second derivatives of the energy and can be obtained in two different ways: (i) using linear response, or (ii) by finite differences. This study uses the latter. The application of this method usually involves several stages to be performed with an acceptable numerical precision. The first problem is to relax the structure to its theoretical equilibrium geometry. The next step is the evaluation of the force constants, which, in finite differences-based methods, are calculated from the variations in the atomic forces which arise for small displacements of the atoms around their equilibrium configuration. This process is usually very time consuming, as it involves $6N$ atomic displacements (where N is the number of atoms in the unit cell) and the corresponding forces evaluation. The calculation of the vibrational frequencies is then fairly straightforward, being given by the eigenvalues of the dynamical matrices. The corresponding eigenvectors provide a representation of the motions of each atom per vibrational mode. In some cases, the normal modes can be depicted in a very simple way, for instance in high frequency stretching modes, but this representation becomes increasingly complicated for lower frequency vibrations, such as librational or bending modes. By correlation of the computed frequencies to the observed spectra, both an assessment of the quality of the calculations and a guide to the assignment of the spectra can be achieved. However, a proper comparison can only be carried out when not only vibrational frequencies but also the corresponding infrared dipole intensities are evaluated. In this case, the comparison between experimental and simulated spectra should be free from ambiguities, even if some frequencies are slightly shifted or the intensities are not exactly matched.

For all our crystal structure calculations, we have used the SIESTA method in the code implementation with the same name. This method has been designed to study the geometry and dynamics of solids and has been applied to the study of ionic[1] and molecular systems[2] and also to metals, semiconductors, or biological systems.[3] The SIESTA code, together with ancillary programs, allows also the calculation of the vibrational frequencies of the normal modes of the solid. We make use here of an extension of the method[4] to evaluate the infrared intensity of each mode, based on the polarization change with the atomic displacements. We also use that information to include in the calculation the long-range field effects that give rise to longitudinal−transverse vibration (LO−TO) splittings.

Nitric acid and nitric acid hydrates are systems of well-accepted atmospheric relevance. They are found in crystalline or aerosol form in clouds both in the troposphere, from where they precipitate in the acid deposition process, and in the stratosphere, where they take part in the chemistry of ozone depletion, in polar stratospheric clouds. Infrared spectra of nitric acid (NA) and nitric acid monohydrate (NAM) crystals have been published by several authors.[5−11] These systems have also been studied from the theoretical point of view in articles that present a refined equilibrium structure of the crystal and the corresponding normal mode vibration analysis.[2,12] However, as far as we know, their simulated infrared spectra have never been published. In the following section of the paper, we describe the theory underlying the calculation of polarization changes

* Corresponding author. E-mail: deliaft@iem.cfmac.csic.es.

10.1021/jp047249d CCC: $27.50
Published on Web 10/26/2004

and infrared intensities. The method is then applied to predict the NA and NAM spectra. The results of the theoretical study are then compared to literature experimental spectra of these systems.

Theory

Technical Details. In this section, we aim to highlight the main technical details used in our calculations on the nitric acid and nitric acid monohydrate systems. More details on the relaxed structures, normal modes, and frequencies for the NA and NAM crystals can be found in previous publications on this subject.[2,12]

Relaxed structures and vibrational properties have been calculated using the SIESTA[13,14] method. The corresponding code is an implementation of density functional theory combined with norm-conserving pseudopotentials to describe the effect of the atomic cores and a linear combination of atomic orbitals as the basis set for the valence electrons. As a result of SIESTA's methodology, the computer time and memory needed are modest, even for systems with many atoms in the unit cell.

In our calculations, we have used the gradient-corrected functional of Perdew, Burke, and Ernzerhof,[15] which provides an accurate treatment of hydrogen bonding and dissociation energies of small molecules. Core electrons are replaced by norm-conserving pseudopotentials of the Troullier−Martins kind, including partial core corrections. The basis set used is a standard split-valence double-ζ with polarization (DZP). The orbitals are spatially confined with a cutoff value of up to 100 meV, which corresponds to the excitation energy arising from the confinement of the basis orbitals. The grid needed in order to calculate the Hartree and exchange-correlation terms has been chosen to have a fineness of 150 Ry. The k grid point sampling has been restricted to the Γ point. The density matrix has been calculated iteratively with a tolerance of 10^{-4}, and the atomic forces for the relaxed structure have been in all cases smaller than 0.04 eV/Å. Tests were run for NAM with a tolerance of 0.02 eV/Å without appreciable changes in the predicted spectrum.

Force constants have been calculated as the numerical derivatives of the analytical interatomic forces with respect to atomic displacements. The displacement has been chosen to be 0.01 Å in all cases. Vibrational frequencies and normal modes have been calculated within the harmonic approximation as the square root of the eigenvalues and as the eigenvectors of the dynamical matrix, respectively. They have been evaluated at the Γ point, the only k point needed for infrared absorption studies.

Infrared Absorption Intensity. The key magnitude for the evaluation of the infrared absorption intensity of a crystal is the macroscopic polarization and, more specifically, its derivatives with respect to atomic displacements. From the polarization, atomic Born charges associated with atomic displacements along the axes can be calculated. In this section, we describe the method we have used to obtain these properties.

Vibrational modes and frequencies have been calculated as described in the previous section. SIESTA has routines to evaluate the macroscopic polarization that are based on the Berry phase method.[16]

The Born effective charge tensor, $Z^*_{ij,\tau}$, is defined[17] as the linear change in the polarization per unit cell created along the direction i when the atom τ is displaced along the direction j

$$Z^*_{ij,\tau} = V\frac{\partial P_i}{\partial r_j^\tau} \tag{1}$$

where V is the volume of the unit cell, P_i is the macroscopic polarization along the i axis, and r_j^τ is the displacement of the atom τ along the j axis.

In this work, Born charges have been evaluated as the numerical derivatives of the polarization per unit cell when displacing each atom along the $+x$, $+y$, and $+z$ axis, corresponding to the crystallographic axis for the present orthorhombic crystals. At this point, it is worth noting that the macroscopic polarization given by the Berry phase method is well-defined modulus, a "quantum" of polarization, i.e., $2e\mathbf{R}$ for a nonmagnetic system, where 2 indicates the occupation, e the electron charge, and $\mathbf{R}$ an arbitrary lattice vector. As we are interested in the increment ΔP_i, we evaluate first P_i at the relaxed atomic positions and then $P_i + \Delta P_i$ with the atom τ displaced a bit along the direction j. In this case, jumps of $2e\mathbf{R}_j$ can occur, so one has to be aware of this possibility and remove these jumps if they do appear. It is also worth noting that there is no need to calculate the Born charge tensors for all atoms in the unit cell but only for the atoms in the irreducible unit. The rest of the Born charges can be deduced using the appropriate space group symmetry. More details are presented in the Discussion section.

We can now address the calculation of the infrared absorption of the crystal. For a molecule in the gas phase, the infrared absorbance of the m normal mode is given by the following expression[18,19]

$$I_{IR}^m = \frac{\rho\pi}{3c}\left|\frac{\partial\vec{\mu}}{\partial Q_m}\right|^2 \tag{2}$$

where ρ is the molecular concentration, c is the velocity of light, $\vec{\mu}$ is the electric dipole moment, and Q_m is the normal mode coordinate

$$U_{j,m}^\tau = Q_m X_{j,m}^\tau \tag{3}$$

Here $U_{j,m}^\tau$ is the m normal mode component of the displacement of the τ atom in the j direction, evaluated from the $X_{j,m}^\tau$ elements of the corresponding vibrational eigenvector.[19] All these equations refer to normal modes that satisfy

$$\sum_{j=1}^{3}\sum_{\tau=1}^{N} M_\tau X_{j,m}^\tau X_{j,n}^\tau = \delta_{mn} \tag{4}$$

where M_τ is the mass of the atom τ.

A similar expression can be used for solid polycrystalline samples, replacing the electric dipole moment by the macroscopic polarization

$$I_{IR}^m \propto \sum_{i=1}^{3}\left(\frac{\partial P_i}{\partial Q_m}\right)^2 \tag{5}$$

where P_i is the i component of the macroscopic polarization and the eigenmodes are calculated at the Γ point.

This expression (eq 5) is valid for solids under two main approximations. First, we suppose that the material is a polycrystal where all directions are equivalent. This is the same as saying that the angle between the crystalline axis and the electric field of the incident infrared light is random. Second, we ignore the effects of the macroscopic shape of the sample, which are mainly transmission−reflection and interference effects. These could be taken into account by constructing a macroscopic electromagnetic model[20] suitable for each specific problem.

The derivative in eq 5 can be rewritten in terms of the Born charges so that the infrared absorbance for the *m* mode results

$$I_{IR}^{m} \propto \sum_{i=1}^{3}\left(\sum_{j=1}^{3}\sum_{\tau=1}^{N} Z^{*}_{ij,\tau} X^{\tau}_{j,m}\right)^{2} \qquad (6)$$

where *N* is the number of atoms in the unit cell.

A further aspect to be considered is the so-called LO−TO splitting, an effect that induces a frequency shifting of some vibrations and which can give rise to significant changes in the infrared spectrum, such as the appearance of new peaks or broadening of some bands. The LO−TO splitting is caused by the macroscopic electric field which appears because of the electrical charge displaced for longitudinal vibrations (LO) in the crystal. These vibrations are thus subject to an electric field which is slightly different to the incident radiation field observed by the transverse vibrations (TO). The modified field induces a blue shift in the corresponding LO frequencies. The inclusion of this treatment in the methodology used in this work has been described in ref 4.

We have used eq 6 to calculate the infrared absorptions of the normal modes of the NAM and NA crystals under study, taking also the LO−TO splitting into account. For a more graphical comparison with the experiment, discussed later in this article, the computed absorptions have been convoluted with a Lorentzian function.

Results and Discussion

Born Charges. *Nitric Acid Monohydrate.* The unit cell of NAM,[21,22] which contains four nitric acid and four water molecules, all of them in ionic form, NO_3^- and H_3O^+, respectively, is represented in Figure 1, where the atom numbering used in this work is also indicated. The crystal has orthorhombic symmetry.

The macroscopic polarization has been calculated as described in ref 13 using the modern theory of polarization.[16] The method needs sampling in k space in order to evaluate a one-dimensional (1D) integral along a given direction of k and then a 2D integral across the corresponding perpendicular plane. From the polarization, Born charges have been calculated in this work using two sampling points for the line integral and one sampling point for the surface integral. In the terminology of ref 23, this is described as 2 × 1 × 1. Convergence of the results has been checked for NAM using grids ranging from 1 × 1 × 1 to 10 × 5 × 5. We have also checked the stability of the Born charges versus the geometry relaxation method used (fixed or relaxed lattice parameters) and versus the basis set, and convergence was achieved in all cases. A variationally optimized basis set[24] with longer cutoff radii and a smoother orbital fallout with growing radius was used for this purpose. The importance of the basis set in the calculation of infrared activities has been noted in the literature.[19] The last check of convergence is related to the sum of the traces of the Born charge matrices for every atom in the unit cell, which is called the acoustic (or neutrality) sum rule, and resulted 0.1 au, a value close enough to 0 to be considered satisfactory.

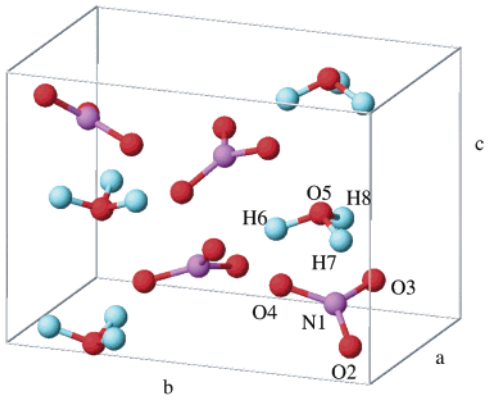

Figure 1. Schematic view of the calculated structure of the unit cell of NAM seen from the *x* axis. The atom numbering is shown for reference in Table 1.

Born effective charge tensors for NAM in atomic units (au) are presented in Table 1 for the atoms in the irreducible unit only. The rest can be deduced using the space group symmetry of NAM ($P2_1cn$).[25] The Born charge tensors can be decomposed into three contributions, an isotropic part, with the same trace as the whole tensor; a symmetric traceless matrix; and an antisymmetric part. In ionic materials, the diagonal element of the isotropic part, $Z^*_{xx,t} = Z^*_{yy,t} = Z^*_{zz,t}$, is the dominant contribution to the Born tensor and is usually close to the formal ionic charge, according to the simple idea of the ions as the elementary parts of the whole solid. In our case, we have atoms attached by covalent bonds instead of ions so that the symmetric contribution to the Born tensor is relevant. The analysis can be pursued by diagonalizing the total symmetric contribution, composed by the isotropic part plus the traceless symmetric matrix. The eigenvectors of this matrix indicate the directional distribution of charges for each atom, and the eigenvalues, the amount of charge that is displaced along each direction. The underlying idea is that bonding directions should be predominant for charge displacements for atoms in a terminal position of the molecule, such as the O atoms in NO_3^-, whereas a larger charge distribution should remain in the plane perpendicular to the symmetry axis for central atoms, such as N in the same system. Diagonalization of the Born charges for NAM yields

TABLE 1: Born Effective Charge Tensors for NAM (au)[a]

		x	*y*	*z*	Q_r	α	bond			*x*	*y*	*z*	Q_r	α	bond
N1	*x*	2.47	0.06	0.75	2.74			O5	*x*	−1.59	0.26	−0.06	−1.61		
	y	−0.77	2.25	0.62	2.58				*y*	−0.32	−1.56	0.10	−1.55		
	z	0.57	0.92	0.88	0.28				*z*	0.01	0.10	−0.65	−0.60		
O2	*x*	−0.95	−0.34	−0.36	−0.84	112	O2−N1	H6	*x*	0.28	−0.48	0.17	0.23	82	H6−O5
	y	−0.23	−1.52	−0.54	−0.30	88			*y*	−0.12	1.94	−0.46	0.35	94	
	z	−0.38	−0.76	−0.73	−2.05	22			*z*	0.03	−0.59	0.52	2.17	8	
O3	*x*	−1.92	0.03	−0.40	−0.84	71	O3−N1	H7	*x*	1.16	0.60	0.25	0.18	79	H7−O5
	y	0.14	−0.81	−0.07	−0.29	88			*y*	0.96	0.83	0.21	0.35	53	
	z	−0.49	−0.14	−0.44	−2.04	19			*z*	0.42	0.19	0.44	1.89	11	
O4	*x*	−1.15	0.45	0.13	−0.80	108	O4−N1	H8	*x*	1.72	−0.63	−0.32	0.24	84	H8−O5
	y	0.56	−1.48	−0.34	−0.31	90			*y*	−0.21	0.36	0.05	0.37	83	
	z	0.27	−0.48	−0.45	−1.97	18			*z*	−0.41	0.14	0.47	1.93	9	

[a] Atoms are numbered as in Figure 1. Q_r represents the eigenvalues of the symmetric component of the Born tensor, and α is the angle (deg) formed by the corresponding eigenvector with the bond shown in the following column.

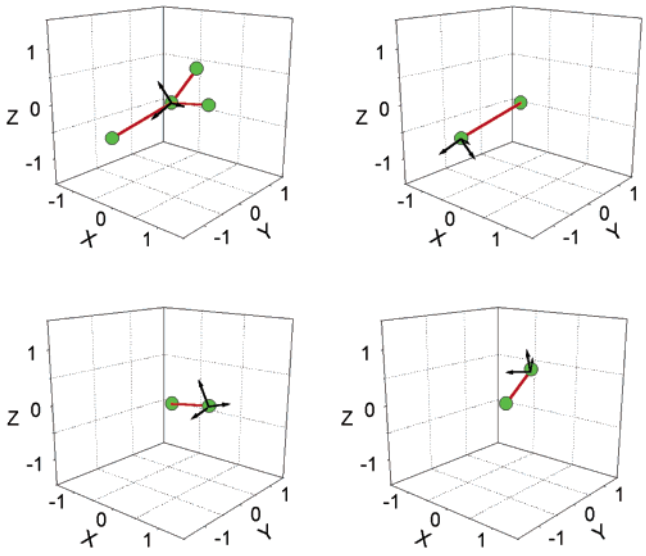

Figure 2. Eigenvectors of the symmetric Born tensor for the NO_3^- group in NAM. Each diagram shows the eigenvectors for one of the atoms and the bond or bonds in which it is involved.

results which comply with the expectations, as reflected in Table 1 for both NO_3^- and H_3O^+ of the irreducible unit. The eigenvalues of the symmetric matrix are listed in Table 1 with the angle that the corresponding eigenvectors form with the bond indicated. The largest eigenvalues are always in the direction closest to that of the appropriate bond for NO_3^- and H_3O^+, with a maximum deviation of 22°. For N and the central O of the H_3O^+ group, however, the minimum charge transfer occurs along the direction closest to the local symmetry axis, and the maximum charge transfer takes place in the perpendicular plane. As an illustration, we represent with arrows in Figure 2 the eigenvectors of the NO_3^- group, and the above commented results can be easily visualized. Therefore, we can conclude that for NAM all molecular bonds determine well-defined charge-transfer directions along which the displacement of charge is greatest in absolute value. The results are approximately equal for all equivalent atoms in each molecular group with negative values for the O atoms in NO_3^- and positive values for the H atoms in H_3O^+.

Nitric Acid. There are 16 NA molecules in the unit cell,[26] also of orthorhombic symmetry, with the disposition represented in Figure 3, which includes the atom numbering for the irreducible unit.

Born charges for NA have also been calculated using a 2 × 1 × 1 k grid. As there are now 80 atoms per unit cell, the calculation is much more time-consuming than it was for NAM. With our computing facilities, namely, a two-processor Sun-Blade 1000 workstation, it took about 10 h to complete the calculation for NAM and around 17 days for pure nitric acid. This is due to the unfavorable scaling in the computation of the macroscopic polarization as opposed to the more favorable scaling in energy computations.

Born effective charge tensors for NA are shown in Table 2 for the four NA molecules that make the irreducible unit. Born charges for the rest of the atoms can be generated from those listed in Table 2 by applying the space group symmetry of NA, $P2_1a$.[27] For NA, the acoustic sum rule has a value of 0.08 au, which again seems satisfactory.

The Born charge tensors have been decomposed into three contributions as described above. The results of the diagonalization of the symmetric part are listed in Table 2. We find a similar behavior as for NAM, with a maximum deviation of

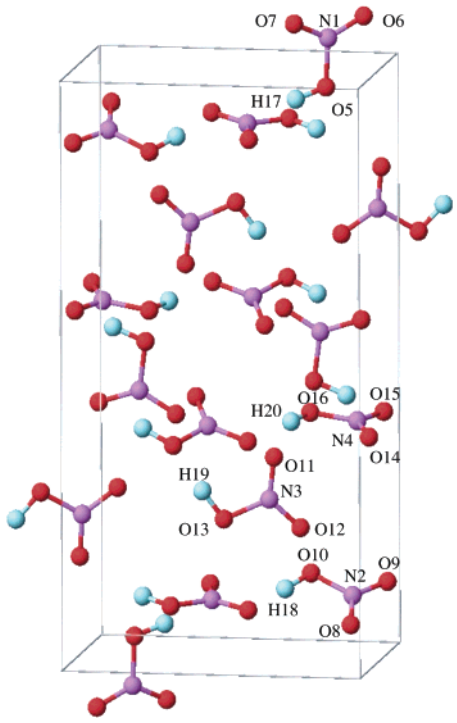

Figure 3. Schematic view of the calculated structure of the unit cell of NA, seen from the *x* axis. The atom numbering is shown for reference in Table 2.

30° from the bonding direction for the O5−H17 atoms. Whereas the charge-transfer values for the N atoms are close to those in NAM, both in magnitude and direction, the charge displacements along the NO bonds, and also those along the OH bonds, have in general smaller values for the terminal atoms than those obtained for the previously described system, although keeping their sign. The conclusion, as before, is that there are well established predominant directions for maximum charge transfer, mainly along the molecular bonds. When comparing NA and NAM crystals, the larger dispersion in $Z^*_{ii,\tau}$ values, and also in the angular distribution of the charge transfers, of the former system can be related to its smaller crystalline symmetry.

Infrared Absorption. *Nitric Acid Monohydrate.* From the optimized geometry of the unit cell and following the theory outlined above, we have calculated the infrared absorption spectrum of NAM. We have also estimated the effect of the LO−TO splitting, making use of the experimental[28] value of the dielectric constant for visible light, $\epsilon_\infty = n_{vis}^2 = 1.54^2 = 2.37$, corresponding to the value of the index of refraction of NAM at visible wavelength, n_{vis}. Both computed spectra are displayed in Figure 4, where a Lorentzian line shape has been assumed with a half-width at a half-maximum (hwhm) value of 15 cm^{-1}. The spectrum shows interesting variations when the LO−TO correction is applied. The main effect consists of a splitting of the stronger peaks of the spectrum, giving rise to resolved independent features which shift in frequency over tens of wavenumbers. This correction therefore induces an appreciable change in the shape of all of the bands of the spectrum.

The computed contour, after LO−TO correction, is compared with previous experimental spectra in Figure 5. For this figure, we have convoluted the calculated intensities with a Lorentzian function of two different widths, 15 cm^{-1} for the peaks at $\nu <$ 2000 and 150 cm^{-1} for those at $\nu >$ 2000 cm^{-1}. The higher frequency region corresponds to O−H stretching vibrations in which the H atoms are involved in strong H bonding, which

TABLE 2: Born Effective Charge Tensors for NA (au)[a]

		x	y	z	Q_r	α	bond			x	y	z	Q_r	α	bond			x	y	z	Q_r	α	bond
N1	x	2.05	−0.36	0.99	2.51			O8	x	−0.76	0.16	0.55	−0.59	95	O8−N2	O15	x	−0.32	0.16	0.34	−0.20	87	O15−N4
	y	−0.38	2.23	0.73	2.57				y	0.07	−0.63	−0.05	−0.15	90			y	0.10	−1.16	−0.37	−0.67	100	
	z	0.76	0.54	1.09	0.30				z	0.44	−0.13	−0.54	−1.20	5			z	0.16	−0.19	−0.76	−1.36	10	
N2	x	1.32	−0.17	−0.96	2.89			O9	x	−0.47	0.27	0.27	−1.95	19	O9−N2	O16	x	−0.28	0.02	0.13	−1.98	20	O16−N4
	y	0.01	2.88	−0.10	2.11				y	0.21	−1.90	−0.11	−0.64	109			y	−0.09	−1.98	0.13	−0.23	88	
	z	−0.83	0.17	1.12	0.32				z	0.23	−0.10	−0.41	−0.18	89			z	0.05	−0.04	−0.42	−0.46	70	
N3	x	1.85	0.17	0.59	2.90			O10	x	−0.41	−0.29	0.20	−0.23	87	O10−N2	H17	x	0.54	−0.16	0.02	0.69	31	H17−O5
	y	0.03	2.89	−0.05	2.19				y	−0.30	−1.63	0.32	−0.45	70			y	−0.21	0.45	−0.13	0.55	93	
	z	0.84	−0.06	0.74	0.39				z	0.15	0.17	−0.39	−1.75	20			z	−0.13	−0.06	0.50	0.26	121	
N4	x	0.65	0.15	−0.93	2.75			O11	x	−1.04	−0.03	−0.35	−0.64	90	O11−N3	H18	x	0.24	−0.21	0.12	0.10	112	H18−O10
	y	0.07	2.68	0.01	2.17				y	0.05	−0.64	0.02	−0.19	92			y	−0.10	1.01	0.12	0.43	83	
	z	−0.45	−0.33	1.95	0.35				z	−0.51	0.02	−0.41	−1.26	2			z	0.12	0.27	0.37	1.09	23	
O5	x	−1.30	0.12	−0.67	−0.29	98	O5−N1	O12	x	−0.65	−0.24	−0.22	−1.69	22	O12−N3	H19	x	0.41	0.66	−0.05	0.08	113	H19−O13
	y	0.21	−0.36	0.07	−0.39	84			y	−0.33	−1.60	−0.07	−0.71	68			y	0.24	1.25	0.13	0.43	100	
	z	−0.44	0.01	−0.65	−1.65	10			z	−0.28	−0.05	−0.34	−0.19	90			z	−0.10	0.40	0.33	1.48	25	
O6	x	−0.68	0.44	−0.12	−1.39	1	O6−N1	O13	x	−0.55	0.02	−0.06	−0.55	72	O13−N3	H20	x	0.36	−0.50	0.00	0.42	96	H20−O16
	y	0.49	−1.08	−0.16	−0.49	89			y	0.26	−1.89	0.11	−0.30	98			y	−0.15	1.47	0.25	0.12	65	
	z	−0.06	−0.07	−0.34	−0.22	89			z	−0.05	0.05	−0.32	−1.91	20			z	0.08	0.70	0.41	1.72	26	
O7	x	−0.53	−0.18	−0.31	−0.57	85	O7−N1	O14	x	−0.42	−0.12	0.50	−0.75	99	O14−N4								
	y	−0.16	−1.22	−0.54	−0.28	92			y	−0.08	−0.80	0.13	−0.28	81									
	z	−0.23	−0.41	−0.67	−1.57	6			z	0.25	0.21	−1.26	−1.45	13									

[a] Atoms are numbered as in Figure 3. Q_r represents the eigenvalues of the symmetric component of the Born tensor, and α is the angle (deg) formed by the corresponding eigenvector with the bond shown in the following column.

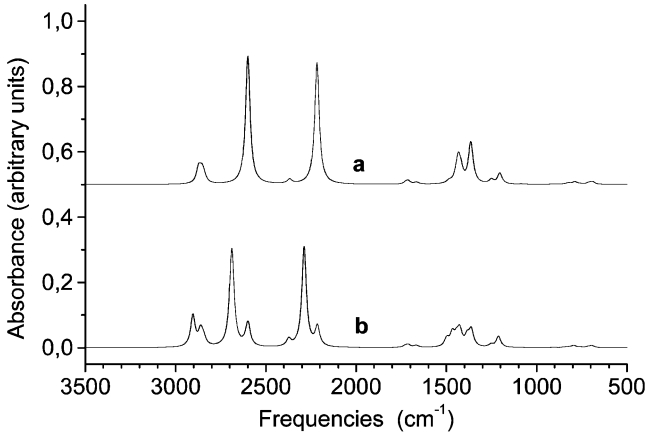

Figure 4. Calculated IR spectrum of NAM (a) without LO−TO correction and (b) with LO−TO correction

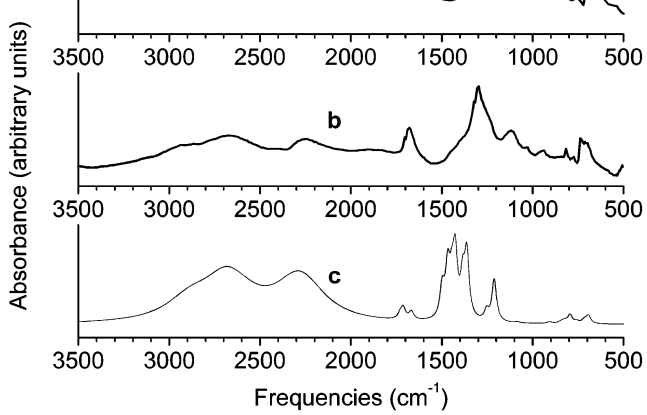

Figure 5. Experimental and calculated infrared absorption spectra of NAM. The spectra are from (a) ref 6, (b) ref 7, and (c) this work.

induces a broadening of the corresponding bands, with respect to similar vibrations when H bonding is not present.[29,30]

There are many articles in the literature dealing with the spectrum of NAM.[6,7,9] From these, we have selected the transmission spectra of Smith et al.[6] (Figure 5a, top), and of Ritzhaupt and Devlin[7] (Figure 5b, middle). Published experimental spectra present some surprising differences which have not been fully explained yet. This effect is frequently found in spectra of this kind of crystalline materials. For those in Figure 5, the major differences appear in the 1000−1500 cm^{-1} range with changes in the relative intensities of the two strong peaks and a shift of the lower frequency one. Smith et al. explain this frequency shift in terms of a loss of symmetry of the nitrate ion, originated by imperfections in the crystal, and no explanation is attempted for the observed intensity change. It is not the purpose of this paper to provide a full justification for these effects, but in our opinion, the intensity variation seems to be too large and peak-selective to be caused by microscopic order−disorder structural changes. The comparison with the ab initio prediction sheds some light on this problem.

Our simulated spectrum (Figure 5c, bottom) presents a reasonable similarity with the experimental spectra and looks closer to spectrum b than to spectrum a. The strongest band in the spectrum, ca. 1400 cm^{-1}, is calculated with a very large intensity relative to the other bands in the prediction, which somehow distorts the comparison with the observed spectra. This band is also blue-shifted with respect to the observations. As noted above, we have carefully checked the convergence of the NAM calculations against the geometry relaxation method and against the basis set, not finding any appreciable changes in frequencies, Born charges, and infrared activities. The shift in the predicted spectrum for this band can be due to any of the approximations in the method (GGA, pseudopotentials, basis set) or more technical reasons. Tests have been performed on the basis set and on the convergence with respect to the different tolerances and other parameters, showing robust results. Further work is needed to ascribe the origin of the deviations, but the present accuracy is enough for this study. The rest of the bands in the spectrum are basically predicted at correct wavenumbers. The lowest frequency band, at 700 cm^{-1}, is assigned as a blend of NO_3^- and H_3O^+ bending vibrations, which in the prediction does not induce large dipole moment displacements, yielding a comparatively low intensity. The band at around 1700 cm^{-1} is split in the calculation, but a composite structure cannot be discarded in the observed spectra as well. The bands calculated over 2000 cm^{-1} agree in location with both a and b spectra.

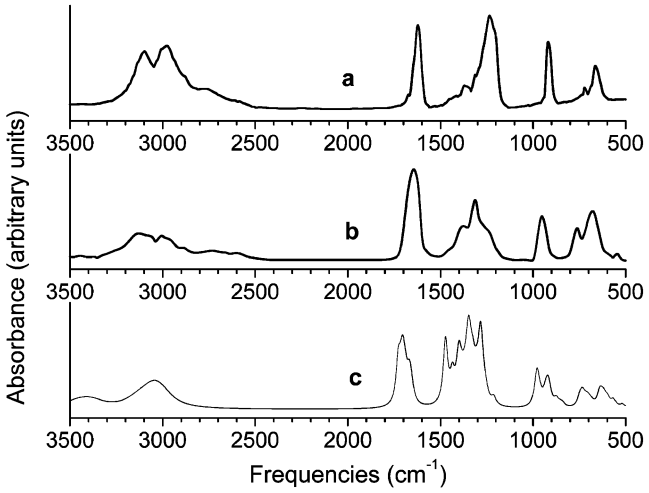

Figure 6. Experimental and calculated IR absorption spectra of NA. The spectra are from (a) ref 8, (b) ref 6, and (c) this work.

Nitric Acid. We have also calculated the infrared spectrum of NA as described above. The value of the dielectric constant for visible light, ϵ_∞, was taken[31] as $\epsilon_\infty = n^2_{vis} = 1.49^2 = 2.22$. The effect of applying the LO−TO correction to the spectrum of the nitric acid crystal was small, and the corrected spectrum only is used for the following discussion.

The infrared spectrum of NA has been reported a few times.[5,6,8] We reproduce in Figure 6 the spectra measured by Koehler et al.[8] (top, part a) and by Smith et al.[6] (middle, part b). These spectra also present some discrepancies in the observed peak intensities. The major differences appear for bands located at either end of the spectral region. Interestingly, whereas the bands at the lower frequency zone are weaker in the spectrum a than those in b, those at the higher-frequency end follow the opposite pattern. The reason for these discrepancies, in our opinion, may lie in small changes in the microscopic structure of the samples due to different methods of preparation of the crystals. Another possibility, relating the observed intensity differences with the temperature at which the spectra were measured, can be discarded on the grounds of the experiments carried out by Smith et al,[6] who recorded spectra at varying temperatures between 113 and 188 K, finding only small changes in the shape of one band, which peaks at about 1300 cm^{-1}.

Considering the discrepancies within experimental spectra, the comparison with the ab initio prediction, Figure 6c, seems satisfactory. The convolution of the calculated intensities has been done as for NAM, with two different broadenings to account for the effect of H bonding with hwhm = 15 cm^{-1} for peaks at $\nu < 2000$ cm^{-1} and hwhm = 75 cm^{-1} for peaks at $\nu > 2000$ cm^{-1}, the latter being smaller than that for NAM, because the hydrogen bonds are weaker in this system. The detailed spectral assignment of the nitric acid spectrum is presented in ref 12. The O−H stretching region presents some small discrepancies, which may arise from different reasons, such as shortcomings of the GGA functional or the lack of inclusion of anharmonicity in the theoretical calculations. The agreement for the rest of the spectrum is quite good, in both frequencies and intensities. The analysis of the spectrum in terms of the theoretical results can provide information to unravel the experimental discrepancies between spectra b and c, if it is assumed that they are due to small microscopic differences between the samples. The lowest frequency band, 700−780 cm^{-1}, corresponds to bending vibrations of the NO_3^- group. The higher intensity in spectrum b can be interpreted in terms of a larger disorder in the relative planes that contain the N−O bonds with respect to the perfect crystal, which has very well-defined layers with the N−O bonds distributed along them. The following band, in the 900−1000 cm^{-1} range, is split in the calculation. The lower frequency peak, at about 870 cm^{-1}, is assigned to the O−H out of plane torsion,[12] and the higher frequency one, at about 980 cm^{-1}, is due to N−O' stretching, where O' represents the oxygen atom bonded to hydrogen. It is possible then that the calculated splitting arises from slight misplacements of the H positions. The band at about 1250−1400 cm^{-1} presents a quite different shape in the experimental spectra, which makes the comparison less meaningful, although the agreement in frequency is quite good. Finally, the peak at about 1650 cm^{-1}, attributed to asymmetric NO_2 stretching, is again in good agreement between prediction and observations.

Conclusions

The SIESTA method, which has proved to be an adequate tool for the study of molecular crystals with many atoms per unit cell, provides also the basis for the calculation of the macroscopic polarization of the crystal. The method has been recently extended to include the determination of Born charges associated with atomic displacements in the normal modes, which can be used to evaluate the infrared intensity of the corresponding vibrations.

We present the application of this formalism to atmospherically relevant species, nitric acid and nitric acid monohydrate crystals. For NAM, the effective Born charges show a highly anisotropic charge distribution, with a negative charge on the O atoms and a positive charge on N. The O−H bond has similar characteristics, with positive charge on the H atoms and negative on the apex O. The corresponding values for NA follow an analogous pattern, with smaller charge concentration in the N−O and O−H bonds.

We have predicted the infrared absorption spectrum of NA and NAM from the corresponding Born tensors and normal mode coordinates. The computed spectra are compared to experimental infrared transmission measurements. The overall agreement can be considered satisfactory.

Acknowledgment. We acknowledge the use of a variationally optimized basis set from M. Fernández-Serra. We are grateful to V. J. Herrero, B. Maté, M. A. Moreno, and I. K. Ortega for frequent discussions. This work has been funded in part by the Spanish Ministry of Science and Technology, Project REN2000-1557. D. Fernández-Torre acknowledges the hospitality of the Earth Sciences Department at Cambridge.

References and Notes

(1) Sainz-Diaz, C. I.; Timón, V.; Botella, V.; Artacho, E.; Hernández-Laguna, A. *Am. Mineral.* **2002**, *87*, 958.

(2) Fernández, D.; Botella, V.; Herrero, V. J.; Escribano, R. *J. Phys. Chem. B* **2003**, *107*, 10608.

(3) See a full list of publications at the SIESTA webpage, http://www.uam.es/departamentos/ciencias/fismateriac/siesta/.

(4) Archer, T. D.; Pruneda, J. M. Unpublished work. Archer, T. D. Ph.D. Thesis, University of Cambridge, 2004. Sanchez-Portal, D.; Souza, I.; Martin, R. M., LCAO Calculation of Dynamical Charges and Ferroelectricity. In *AIP Conference Proceedings*; Cohen, R. E., Ed.; American Institute of Physics: Melville, New York, 2000, 535, 111−120 (Fundamental Physics of Ferroelectrics 2000).

(5) McGraw, G. E.; Bernitt, D. L.; Hisatsune, I. C. *J. Chem. Phys.* **1965**, *42*, 237.

(6) Smith, R. H.; Leu, M.-T.; Keyser, L. F. *J. Chem. Phys.* **1991**, *95*, 5924.

(7) Ritzhaupt, G.; Devlin, J. P. *J. Phys. Chem.* **1991**, *95*, 90.

(8) Koehler, B. G.; Middlebrook, A. M.; Tolbert, M. A. *J. Geophys. Res.* **1992**, *97*, 8065.

(9) Toon, O. B.; Tolbert, M. A.: Koehler, B. G.; Middlebrook, A. M.; Jordan, J. *J. Geophys. Res.* **1994**, *99*, 25631.
(10) Koch, T. G.; Homes, N. S.; Roddis, T. B. and Sodeau, J. R. *J. Chem. Soc., Faraday Trans.* **1996**, *92*, 4787.
(11) Escribano, R.; Couceiro, M.; Gómez, P. C.; Carrasco, E.; Moreno, M. A.; Herrero, V. J. *J. Phys. Chem. A* **2003**, *107*, 651.
(12) Ortega, I. K.; Escribano, R.; Fernández, D.; Herrero, V. J.; Maté, B.; Medialdea, A.; Moreno, M. A. *Chem. Phys. Lett.* **2003**, *378*, 218.
(13) Ordejón, P.; Artacho, E. and Soler, J. M. *Phys. Rev. B: Condens. Matter Mater. Phys.* **1996**, *53*, R10441.
(14) Soler, J. M.; Artacho, E.; Gale, J. D.; García, A.; Junquera, J.; Ordejón, P.; Sánchez-Portal, D. *J. Phys.: Condens. Matter* **2002**, *14*, 2745.
(15) Perdew, J. P.; Burke, K.; Ernzerhof, M. *Phys. Rev. Lett.* **1996**, *77*, 3865.
(16) King-Smith, R. D.; Vanderbilt, D. *Phys. Rev. B: Condens. Matter Mater. Phys.* **1993**, *47*, 1651.
(17) Gonze, X.; Lee, C. *Phys. Rev. B: Condens. Matter Mater. Phys.* **1997**, *55*, 10355.
(18) Wilson, E. B.; Decius, J. C.; Cross, P. C. *Molecular Vibrations*; McGraw-Hill: New York, 1955.
(19) Porezag, D.; Pederson, M. R. *Phys. Rev. B: Condens. Matter Mater. Phys.* **1996**, *54*, 7830.
(20) Balan, E.; Saitta, A. M.; Mauri, F.; Calas, G. *Am. Mineral.* **2001**, *86*, 1321.
(21) Delaplane, R. G.; Taesler, I.; Olovsson, I. *Acta Crystallogr.* **1975**, *B31*, 1486.
(22) Lebrun, N.; Mahe, F.; Lamiot, J.; Foulon, M.; Petit, J.; Prevost, D. *Acta Crystallogr.* **2001**, *B57*, 27.
(23) Xinyuan Zhao; Vanderbilt, D. *Phys. Rev. B: Condens. Matter Mater. Phys.* **2002**, *65*, 75105.
(24) Anglada, E.; Soler, J. M.; Junquera, J.; Artacho, E. *Phys. Rev. B: Condens. Matter Mater. Phys.* **2002**, *66*, 205101.
(25) For the second unit (N9, ..., H16), the elements with $i, j = 1, 2; 1, 3; 2, 1;$ and $3, 1$ of Z^* change sign; also the elements $1, 2; 2, 1; 2, 3;$ and $3, 2$ of the third unit (N17, ..., H24) change sign, and so do the $1, 3; 2, 3; 3, 1;$ and $3, 2$ elements of the forth unit (N25, ..., H32).
(26) Luzzati, V. *Acta Crystallogr.* **1951**, *4*, 120.
(27) For the second unit (N21, ..., H40), there are no sign changes in any Z^* elements; on the contrary, for the third (N41, ..., H60) and the forth units (N61, ..., H80), the $1, 2; 2, 1; 2, 3;$ and $3, 2$ elements of Z^* change sign.
(28) Berland, B. S.; Haynes, D. R.; Foster, K. L.; Tolbert, M. A.; George, S. M.; Toon, O. B. *J. Phys. Chem.* **1994**, *98*, 4358.
(29) *The Hydrogen Bond*; Shuster, P., Zundel, G., Sandorfy, G., Eds.; North-Holland: Amsterdam, 1976; Vols. I−III.
(30) *Molecular Interactions*; Ratajczak, M., Orville-Thomas, W. J., Eds.; Wiley: New York, 1980.
(31) Middlebrook, A. M.; Berland, B. S.; George, S. M.; Tolbert, M. A. *J. Geophys. Res.* **1994**, *99*, 25665.